JOURNAL OF THERMOPHYSICS AND HEAT TRANSFER
Vol. 7, No. 4, Oct.-Dec. 1993

Rocket Plume Radiation Base Heating by Reverse Monte Carlo Simulation

John Everson*
REMTECH, Inc., Huntsville, Alabama 35805
and
H. F. Nelson†
University of Missouri—Rolla, Rolla, Missouri 65401

A reverse Monte Carlo radiative transfer code is developed to predict rocket plume base heating. It is more computationally efficient than the forward Monte Carlo method, because only the radiation that strikes the receiving point is considered. The method easily handles both gas and particle emission and particle scattering. Band models are used for the molecular emission spectra, and the Henyey-Greenstein phase function is used for the scattering. Reverse Monte Carlo predictions are presented for 1) a gas-only model of the Space Shuttle main engine plume; 2) a pure scattering plume with the radiation emitted by a hot disk at the nozzle exit; 3) a nonuniform temperature, scattering, emitting, and absorbing plume; and 4) a typical solid rocket motor plume. The reverse Monte Carlo method is shown to give good agreement with previous predictions. Typical solid rocket plume results show that 1) CO_2 radiation is emitted from near the edge of the plume; 2) H_2O gas and Al_2O_3 particles emit radiation mainly from the center of the plume; and 3) Al_2O_3 particles emit considerably more radiation than the gases over the 400–17,000-cm^{-1} spectral interval.

Nomenclature

a_D = Doppler broadening fine-structure parameter
a_L = Lorentz broadening fine-structure parameter
c = mole fraction
d = line spacing, cm^{-1}
$d\Omega$ = elemental solid angle, sr
FOV = field of view
g = asymmetry factor
I = radiative intensity, W/(cm^2-sr-cm^{-1})
I_b = Planck blackbody function, W/(cm^2-sr-cm^{-1})
i_g = total number of gases
i_p = total number of particle sizes
k = band model absorption coefficient, cm^{-1}
N = number of rays
n = particle number density, cm^{-3}
n_{ij} = exponent in broadening parameter for gas i due to gas j
P = total pressure, atm
P_{HG} = Henyey-Greenstein scattering phase function
q_ω = radiative flux, W/(cm^2-cm^{-1})
RAN = random number, uniformly distributed between 0–1
s = distance along ray path, cm
T = temperature, K
u = band model optical depth
X_D = Doppler line parameter
X_L = Lorentz line parameter
y = collisional plus Doppler optical depth of gas
α_g = gas absorption coefficient, cm^{-1}
α_p = particle absorption coefficient, cm^{-1}
γ_D = half-width due to Doppler broadening, cm^{-1}
γ_{ii} = line self-broadening parameter for gas i
γ_{ij} = line-broadening parameter, gas i due to gas j
γ_L = half-width due to collision broadening, cm^{-1}
η_p = particle scattering coefficient, cm^{-1}
θ = polar scattering angle
σ_{abs} = particle absorption cross section, cm^2
σ_{ext} = particle extinction cross section, cm^2
σ_{sca} = particle scattering cross section, cm^2
τ = optical depth
ϕ = azimuthal scattering angle
ω = wave number, cm^{-1}

Subscripts

CG = Curtis-Godson approximation
i = gas, or particle species
ω = wave number

Superscript

$-$ = square root average over wave band

Introduction

An advanced solid rocket motor (ASRM) is being developed to increase the payload capability of the Space Shuttle. The ASRM has a higher performance propellant than the current Space Shuttle solid rocket boosters. This increased performance, due mainly to increased aluminum loading, will increase the plume temperature and, in turn, the plume radiative emission and the Shuttle base heating. Since the exhaust plume of the ASRM contains a large number of particulates with high albedos, appreciable radiation scattering occurs within the plume. This scattering must be modeled accurately in the radiative transfer calculation in order to obtain a reasonable estimate of the base heating. Current methods for predicting radiative base heating do not adequately account for the effects of radiation scattering. Consequently, improved radiative base heating predictive methods must be developed.

Several codes currently exist that calculate the radiation from a rocket plume. The codes GASRAD[1] and SIRRM[2–4] use a band model treatment for the calculation of radiation

---

Received Dec. 22, 1992; presented as Paper 93-0138 at the AIAA 31st Aerospace Sciences Meeting and Exhibit, Reno, NV, Jan. 11–14, 1993; revision received March 10, 1993; accepted for publication March 11, 1993.

*Principal Scientist.

†Professor of Aerospace Engineering, Thermal Radiative Transfer Group, Department of Mechanical and Aerospace Engineering and Engineering Mechanics. Associate Fellow AIAA.

from the gas in the rocket plume; however, only SIRRM has the capability to include the effects of particulates on the plume radiation. For studies concerning infrared radiation, the only significant scattering is due to particulates in the plume. In SIRRM, scattering is treated using two- and six-flux models. In the two-flux model the particulates scatter and radiate only forward and backward along the line-of-sight. The six-flux model includes scattering and emission along two additional orthogonal directions perpendicular to the line-of-sight. Thus, the treatment of the scattering and emission of radiation by particles is limited. In reality, SIRRM was developed to predict radiation signatures with the plume viewed from infinity, so it is not directly applicable to heat transfer predictions where the plume is close to the heated surface.

Watson and Lee[5,6] developed a code for prediction of base heating based on a forward Monte Carlo method; however, it considers only the gray gas and gray particle case, and only one particle size is allowed. Pearce et al.[7] developed a base heating code based on the standard plume flowfield (SPF-II)[8] and SIRRM-II,[4] and achieved good agreement with experimental results from a subscale, solid rocket motor plume. The longer wavelength infrared spectra were very accurately predicted; however, large errors occurred at short wavelengths where most of the heating occurred. They concluded that careful, extensive measurements of base heating are needed, including not only spatially and spectrally resolved plume radiances, but also plume gas dynamic and optical properties, and that careful and detailed validations of numerical codes against these measurements are required.

Forward Monte Carlo methods trace numerous energy bundles, beginning at the source of radiation, through whatever scattering events take place, until the bundles escape from the plume, where they either hit or miss the surface whose heating is being studied. They have the capability to correctly predict the effects of scattering on the transfer of radiation and accurately predict the radiative heating. Nongray molecular spectra are usually modeled on a line-by-line basis. Unfortunately, a large fraction of the bundles of energy leaving the plume miss the surface being studied and do not contribute to the surface heating rate. These wasted energy bundles increase the computer time required for accurate calculations. The reverse Monte Carlo approach can overcome this problem and increase computer efficiency.[9,10]

There remains a need to develop a base heating code that can accurately represent the effects of scattering, permit a spectral treatment of the radiation transfer, handle multiple particle sizes, and can do so in a computationally efficient manner.[11] This article describes the reverse Monte Carlo approach to the calculation of base heating due to a rocket plume that contains particulates that emit and scatter radiation. The approach is capable of calculating the spectral heating rate, handling multiple particle sizes, treating the effects of scattering (both isotropic and anisotropic) on the propagation of radiation through the rocket plume, and is computationally efficient. It requires a detailed knowledge of the properties at each point in the plume flowfield, including the gas temperature, gas pressure, and mole fraction of all the gases present, and the temperature, number density, and radius of each type of particle present. Several sizes for each particle type are also possible. Currently, atmospheric effects are not considered; however, the method can be easily extended to account for them. The accuracy of the prediction is limited by the accuracy of the plume flowfield prediction and the optical properties used. It is very easy to upgrade to better particle optical properties as they become available.

Reverse Monte Carlo Method

The reverse Monte Carlo method for the calculation of base heating of a rocket due to radiation emitted in its plume is developed assuming that the plume flowfield properties are known. Typically, the plume flowfield is calculated using the SPF-II code.[8] A schematic of the reverse Monte Carlo method applied to the heating of a point on a surface and an outline of the numerical procedure is shown in Fig. 1. It shows rays emitted backwards in time from the surface point (located at 1) to the plume. Some of the rays are absorbed in the plume. Some of the rays are scattered into the nozzle where they are absorbed, either by the gases or particles in the nozzle, or by the nozzle walls. The rays are assumed to be emitted at the point where they are absorbed, and then to retrace their incident path forward in time back to the surface point and contribute to the heating process. Rays emitted from the nozzle gases, particles, and walls contribute to the searchlight radiation.

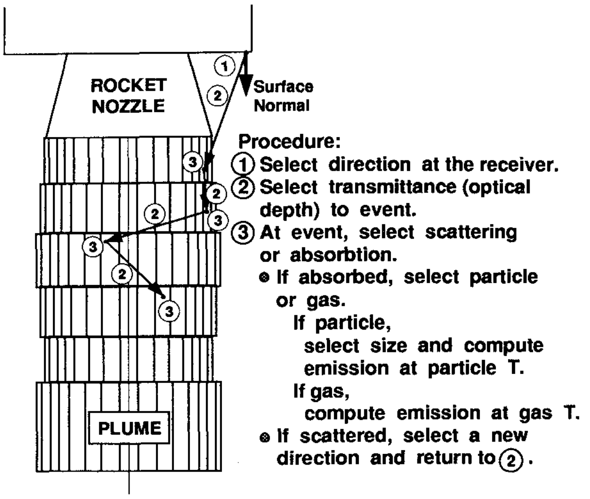

Fig. 1 Schematic of rocket plume and reverse Monte Carlo methodology.

The radiative flux at a point on a surface (as measured by a sensor) is defined as

$$q_\omega = \int_{\mathrm{FOV}} I_\omega \cos\theta \, \mathrm{d}\Omega \tag{1}$$

where I_ω is the specific intensity of the radiation (radiance) entering the sensor's FOV, and θ is the polar angle between the radiation intensity direction and the normal to the receiving surface. Hereafter, the subscript ω, representing the radiation spectral variation, will be dropped to simplify the notation. The integral is evaluated numerically by sending out a large number of rays at random angles within the field of view and determining the value of $I \cos\theta$ for each ray. These values are summed and the result is divided by the total number of rays. This gives the average value of $I \cos\theta$ over the FOV. The integral in Eq. (1) is then found from

$$\langle I \cos\theta \rangle_{\mathrm{FOV}} = \frac{\sum_N I \cos\theta}{N} = \frac{\int_{\mathrm{FOV}} I \cos\theta \, \mathrm{d}\Omega}{\int_{\mathrm{FOV}} \mathrm{d}\Omega} \tag{2}$$

where $\langle\ \rangle$ indicates an average value.

The direction of the ray sent out from the surface is determined by θ, and ϕ (step ① of Fig. 1). These angles are determined by picking two random numbers (RAN) with values between 0–1. Therefore, from the definition of the solid angle FOV

$$\mathrm{RAN} = \frac{\int_0^{\theta} \sin\theta' \, \mathrm{d}\theta'}{\int_0^{\theta_{\max}} \sin\theta' \, \mathrm{d}\theta'} \tag{3}$$

where $\theta_{\max}$ is the half-angle of the conical shaped FOV and

$$\mathrm{RAN} = \phi/(2\pi) \tag{4}$$

Equations (3) and (4) yield the values of θ and ϕ in terms of RAN. By choosing θ and ϕ in this manner, the rays leaving the surface sample the entire FOV without biasing one region over another. An unbiased sampling of $I \cos \theta$ over the field of view is necessary so that $\Sigma_N I \cos \theta$ properly represents the integral in Eq. (1).

The value of I is determined from the plume properties at the radiative emission point (backward ray absorption point). This is done by following the ray backward in time from the receiving surface through the rocket plume from event to event until an absorption takes place (see Fig. 1). There are two possible events: 1) the ray is absorbed by the gases or particulates, or 2) the ray is scattered by the particulates.

The distance, Δs, along the ray between events (step ② of Fig. 1) is determined from

$$\mathrm{RAN} = \exp(-\Delta\tau) \tag{5}$$

where $\Delta\tau$ is the change in optical depth (evaluated along s) in the plume between events. $\Delta\tau$ is a function of distance Δs, along the ray. The total optical depth (τ) is the sum of the optical depths of the gases and the particles, and it is determined from the optical properties of the rocket plume as will be discussed later. The value of Δs is determined from Eq. (5) in terms of RAN. It, together with the direction of the ray, determines the coordinates of the point where an event occurs.

Whether or not the event is a scattering or an absorption is determined by choosing a value for RAN and comparing it to the local albedo (step ③ of Fig. 1). If RAN is less than or equal to the albedo, the ray is scattered, otherwise it is absorbed. The albedo is related to the total absorption and scattering coefficients [albedo $= \eta_p/(\alpha_g + \alpha_p + \eta_p)$]. The total absorption coefficient is the sum of the individual absorption coefficients of the gases and the particles ($\alpha_g + \alpha_p$). The absorption coefficient of each gas present in the plume ($\alpha_{g_i} = k_i c_i P$) is evaluated using band modeling, which will be discussed later. The absorption coefficient of the particles is $\alpha_p = \Sigma_{i=1}^{i_p} n_i \sigma_{\mathrm{abs}_i}$, and for the gases it is $\alpha_g = \Sigma_{i=1}^{i_g} k_i c_i P$. Similarly, the total scattering coefficient is $\eta_p = \Sigma_{i=1}^{i_p} n_i \sigma_{\mathrm{sca}_i}$.

When a scattering event occurs, a new direction must be chosen for the ray. Since the scattering phase function, which determines the direction of scattering, will be different for each particle size (the particles are distributed by sizes according to diameters and type in the SPF-II flowfield[8]), it is necessary to determine which size particle does the scattering. This is done by choosing a value for RAN and comparing it to the ratio of partial scattering coefficients

$$\mathrm{RAN} \leq \sum_{i=1}^{j} n_i \sigma_{\mathrm{sca}_i} / \eta_p \tag{6}$$

The sum in the numerator is over only the first j lowest particle sizes. The index j in the above ratio is increased until the ratio is greater than or equal to RAN. The value of j for which this occurs gives the particle size that scatters the ray. The new polar angle of the ray, defined with respect to the ray's original direction, is determined by

$$\mathrm{RAN} = \frac{\int_0^{\theta} P_{\mathrm{HG}_j}(\theta') \sin \theta' \, \mathrm{d}\theta'}{\int_0^{\pi} P_{\mathrm{HG}_j}(\theta') \sin \theta' \, \mathrm{d}\theta'} \tag{7}$$

where $P_{\mathrm{HG}_j}(\theta)$ is the Henyey-Greenstein scattering phase function for the jth particle size. The new azimuthal angle of scattering (ϕ) is given by Eq. (4).

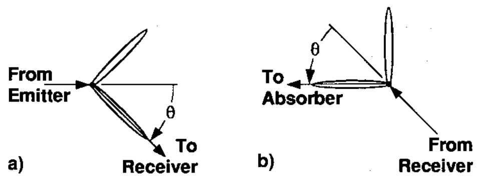

Fig. 2 Scattering phase function: a) forward phase function and b) reverse phase function.

The Henyey-Greenstein phase function is given by

$$P_{\mathrm{HG}_j}(\theta) = \frac{1 - g_j^2}{4\pi(1 + g_j^2 - 2g_j \cos \theta)^{3/2}} \tag{8}$$

where g_j is the asymmetry factor for the jth particle size, which is calculated using Mie theory. It is a function of the particle size, the particle complex index of refraction, and the wave number.

The scattering phase function is defined for rays propagating in the forward direction, not the reverse direction. The phase function for a ray propagating in the reverse direction is the same as the phase function for a ray propagating in the forward direction when it is referenced with respect to the ray direction prior to scattering. This can be shown by the following argument. A ray propagating in the forward direction (from plume to receiver), according to a phase function shown in Fig. 2a, will scatter principally in the θ direction. The reverse phase function (ray propagating from receiver to plume) is shown in Fig. 2b. It is the same as the forward phase function, but defined with respect to the direction of the reverse ray. A ray propagating in the reverse direction travels as shown in Fig. 2b. The reverse ray will be scattered into the θ direction, since the incident and scattered rays have an angle θ between them. Consequently, the forward ray exactly backtracks the reverse ray path as it traverses the scattering event.

After a number of scatterings, the ray may be absorbed. The absorption location determines the value for I in Eq. (2). It is necessary to determine whether the ray is absorbed by the gas or by the particles, because the gas and each of the particle size groups will usually have different temperatures. This is done in terms of the local absorption coefficient and RAN, using the relation

$$\mathrm{RAN} \leq \frac{\sum_{i=1}^{j} n_i \sigma_{\mathrm{abs}_i}}{\alpha_g + \alpha_p} \tag{9}$$

The index j is increased until Eq. (9) is satisfied, or until $j = i_p$. The value of j when Eq. (9) is satisfied determines the size of the particle that absorbs the ray. If Eq. (9) is not satisfied when $j = i_p$, the ray is absorbed by the gas. The value of I assigned to the ray is given by the Planck blackbody function evaluated at the temperature of the gas or the particle. If the ray is scattered out of the plume, the value of I is zero.

Application to Rocket Plumes

The plume flowfield is assumed to be axially symmetric as shown schematically in Fig. 1. It is divided into axial sections, each of which is divided into several radial sections creating concentric cylindrical volumes with boundaries midway between the flowfield solution points. The properties in each volume (pressure, temperature, and mole fractions of the gas species, and the number densities and temperatures for each of the particle sizes) are assumed to be constant.

Gas Optical Properties

The spectral properties of the plume gases are treated using the random band model with an exponential-line-strength distribution.[12] This band model assumes that the line strengths of the gas bands are given by an exponential-line-strength distribution function. The effects of Lorentz and Doppler broadening are both included in the model. The optical depth of the gases is given by

$$\tau = \sum_{i=1}^{ig} k_i u_i \sqrt{1 - 1/\sqrt{y_i}} \tag{10}$$

with

$$y_i = \{1 - [X_{L_i}/(k_i u_i)]^2\}^{-2} + \{1 - [X_{D_i}/(k_i u_i)]^2\}^{-2} - 1 \tag{11}$$

where $u_i = Pc_i s$, and where s is the total path length in the plume. The Lorentz (collision) broadening optical depth parameters X_{L_i} and a_{L_i} are given for each gas species as

$$X_{L_i} = \frac{k_i u_i}{\sqrt{1 + k_i u_i/(4a_{L_i})}} \tag{12}$$

$$a_{L_i} = \gamma_{L_i} d_i \tag{13}$$

with

$$\gamma_{L_i} = P\left[c_i \gamma_{ii} \left(\frac{273}{T}\right)^{n_{ii}} + \sum_j c_j \gamma_{ij} \left(\frac{273}{T}\right)^{n_{ij}}\right] \tag{14}$$

where γ_{ii}, γ_{ij}, n_{ii}, and n_{ij} are constants given in Refs. 2 and 12, P is the gas pressure, and T is the gas temperature. The absorption coefficient k_i (cm^{-1} at 1 atm and the local T) and spectral line spacing parameter d_i are the fundamental optical parameters for each gas i, and are determined from Refs. 2 and 12.

The Doppler broadening optical depth parameters are

$$X_{D_i} = 1.70(\gamma_{D_i}/d_i)\sqrt{\ln[1 + (k_i u_i/1.70a_{D_i})^2]} \tag{15}$$

$$\alpha_{D_i} = \gamma_{D_i}/d_i \tag{16}$$

with

$$\gamma_{D_i} = 0.3581 \times 10^{-6}\omega\sqrt{(T/M_i)} \tag{17}$$

where ω is the wave number of the radiation and M_i is the molecular weight of gas i (g/g-mole).

Homogeneous Plumes

Since thermal radiation is contained in a wide spectral band, it is necessary to perform the Monte Carlo calculations over a wave band rather than at a single wave number. It has been found for heat transfer calculations which neglect the atmosphere, that wavebands as large as 400 cm^{-1} yield results with satisfactory accuracy when the band model parameters are square-root averaged over the wave band (Ref. 12, p. 345). This is done by replacing k, d, and ω in Eqs. (10–17) by their wave band average. No changes in the functional form of Eqs. (10–17) are necessary. The wave band averages are

$$\bar{k} = \left[\frac{\int_{\Delta\omega} I_b(\omega, T)\sqrt{k(\omega, T)}\, d\omega}{\int_{\Delta\omega} I_b(\omega, T)\, d\omega}\right]^2 \tag{18}$$

$$\frac{1}{\bar{d}} = \left[\frac{\int_{\Delta\omega} I_b(\omega, T)\sqrt{\dfrac{k(\omega, T)}{d(\omega, T)}}\, d\omega}{\int_{\Delta\omega} I_b(\omega, T)\sqrt{k(\omega, T)}\, d\omega}\right]^2 \tag{19}$$

$$\bar{\omega} = \frac{\int_{\Delta\omega} I_b(\omega, T)\omega\, d\omega}{\int_{\Delta\omega} I_b(\omega, T)\, d\omega} \tag{20}$$

where $\Delta\omega$ is the bandwidth. These band model equation modifications are only valid for homogeneous gases.

Nonhomogeneous Plumes

For an inhomogeneous gas, Eqs. (10–17) are modified using the Curtis-Godson approximation. The values for $\bar{k}$, a_D, and a_L, that are used in Eqs. (10–17), are replaced by path-averaged quantities[2,13]

$$\bar{k}_{\mathrm{CG}} = \frac{\int_0^s \bar{k}(\Delta\omega, s')c(s')P(s')\, ds'}{\int_0^s c(s')P(s')\, ds'} \tag{21}$$

$$a_{L_{\mathrm{CG}}} = \frac{\int_0^s \bar{k}(\Delta\omega, s')c(s')P(s')a_L(\Delta\omega, s')\, ds'}{\int_0^s \bar{k}(\Delta\omega, s')c(s')P(s')\, ds'} \tag{22}$$

$$a_{D_{\mathrm{CG}}} = \frac{\int_0^s \bar{k}(\Delta\omega, s')c(s')P(s')a_D(\Delta\omega, s')\, ds'}{\int_0^s \bar{k}(\Delta\omega, s')c(s')P(s')\, ds'} \tag{23}$$

Particle Optical Properties

The particles in the plume are assumed to be spherical and homogeneous; therefore, their optical properties can be determined from Mie theory. The complex index of refraction of the Al_2O_3 particles is given in Ref. 2, pp. 101–106. The required optical properties of the particles are the extinction, absorption, and scattering cross sections, and g (average value of the cosine of the scattering angle). The extinction optical depth of the particles is given by

$$\tau = \int_0^s \left[\sum_{i=1}^{ip} n_i \sigma_{\mathrm{ext}_i}\right] ds \tag{24}$$

where, $\sigma_{\mathrm{ext}} = \sigma_{\mathrm{abs}} + \sigma_{\mathrm{sca}}$.

Since the heat flux is calculated for a wave band rather than at a single value of ω, it is necessary to calculate the wave band average for the optical cross sections, and for g. This is done using a Planck-weighted average. For example the average value of g is

$$\bar{g} = \frac{\int_{\Delta\omega} g(\omega)I_b(\omega, T)\, d\omega}{\int_{\Delta\omega} I_b(\omega, T)\, d\omega} \tag{25}$$

Similar calculations are done for the optical cross sections σ_{ext}, σ_{abs}, and σ_{sca}.

Results and Discussion

Validation of Reverse Method

Two test cases were used to validate the reverse Monte Carlo approach. The first case was to predict the radiant heat flux from a Space Shuttle main engine (SSME) plume, which contains only gas species. The second case was to predict the radiative heating from a blackbody disk located at the base of a pure scattering plume, to a point 30 cm from the disk's center and in the plane of the disk.

The first case was used to compare predictions between GASRAD and the reverse Monte Carlo method to verify the implementation of the band model in the Monte Carlo code. The case simulated measurements made during a static test of the SSME. The SSME has a regeneratively cooled nozzle with an area ratio of 77 and an exit diameter of 230 cm. During the test it was operating at a chamber pressure of 20.7 MPa (3000 psia) and a mixture ratio of 6 (O_2/H_2). Because the plume is overexpanded at sea level, there was a strong Mach disk about 150 cm from the exit. The heat flux was calculated for two sensors mounted on a static test stand, which was located 305 cm radially outward from the plume centerline near the engine nozzle exit plane.[14] Each sensor had a 60-deg FOV. One sensor looked across the plume 18-cm downstream of the nozzle exit, the other looked downstream into the plume at a 30-deg angle as shown in Fig. 3. The reverse Monte Carlo and GASRAD predictions are shown in Table 1 for a wave band from 1000 to 9800 cm^{-1}. The agreement between the two methods is very good. Both the average value and the standard deviation of the reverse Monte Carlo method are given in Table 1. The deviation in the Monte Carlo result is due to the statistical error of the Monte Carlo procedure. The average and standard deviation were determined by running the Monte Carlo program several times using different random number sequences.

The second test case was designed to test the ability of the reverse Monte Carlo approach to handle isotropic and anisotropic scattering. It considered the scattering of radiation emitted by a 20-cm-diam, 2000 K, blackbody disk at the base of a cylindrical plume of particles as shown in Fig. 4. The receiver was located in the plane of the disk 30-cm radially outward from the center of the disk and had an unrestricted FOV (2π sr). The cylinder and disk were equal in diameter and the cylinder height was five times the diameter. The particles were pure scatterers (albedo equal 1); hence, they did not emit any radiation. The number density and scattering cross section of the particles were chosen so that the extinction coefficient was 0.05 cm^{-1}. Three cases were considered. Case 1 assumed the disk to be a diffuse emitter and the particles to be isotropic scatterers. Case 2 assumed the disk to be a diffuse emitter and the particles to be anisotropic scatterers. The phase function for the scattering angle was chosen so that about 24% of the rays scattered in the rear hemisphere (g = 0.38). The number density and scattering cross section of the particles were chosen so that each ray that hit the emitting disk was scattered an average of 1.52 times in the reverse Monte Carlo treatment of the problem. This low number of scatterings was chosen because it is thought that a large number of anisotropic scatterings will approach the isotropic scattering result. Therefore, this case demonstrates the validity of using the scattering phase function defined for a forward procedure as the phase function for the reverse Monte Carlo procedure. Case 3 was the same as case 1, except that the emission from the disk was focused to a 60-deg (full angle) cone. In each of these cases, the radiative heat flux to the

Table 1 Comparison of reverse Monte Carlo and GASRAD predictions

	Flux, W/(cm^2)	
	GASRAD	Reverse Monte Carlo
Normal aspect	2.05	2.13 ± 0.02
30-Deg aspect	6.38	6.33 ± 0.09

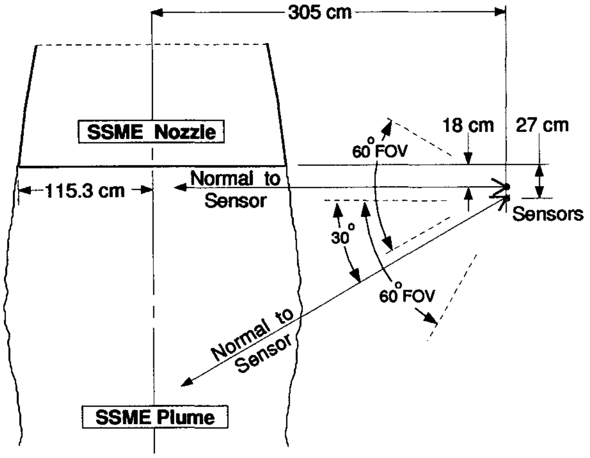

Fig. 3 Schematic of pure gaseous SSME plume and sensor locations.

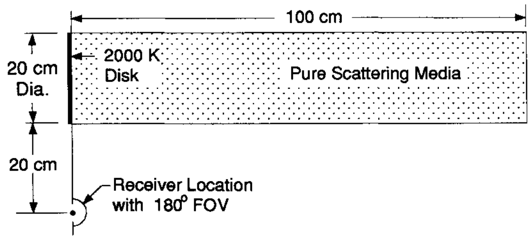

Fig. 4 Pure scattering plume model and receiver location.

Table 2 Comparison of forward and reverse Monte Carlo predictions

	Flux, W/(cm^2)	
	Forward Monte Carlo	Reverse Monte Carlo
Case 1		
Diffuse emitter, isotropic scattering	0.226 ± 0.021	0.235 ± 0.006
Case 2		
Diffuse emitter, anisotropic scattering	0.188 ± 0.015	0.182 ± 0.007
Case 3		
Nondiffuse emitter, isotropic scattering	0.284 ± 0.021	0.271 ± 0.014

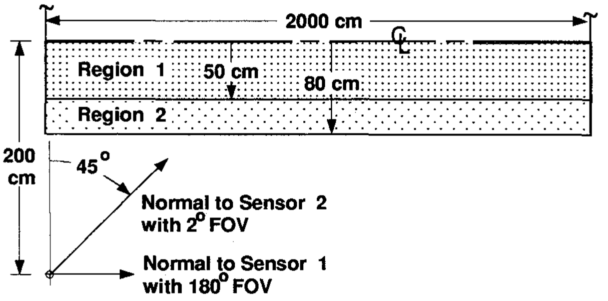

Properties	Region 1	Region 2
Pressure (atm)	1	1
Temperature (K)		
Gas	2500	2000
1 μm radius particles	2500	2000
5 μm radius particles	3000	2400
Gas mole fraction		
H2O	0.2	0.2
CO2	0.1	0.1
Particle num density (cm^{-3})		
1 μm radius particles	10^6	10^6
5 μm radius particles	10^4	10^4

Predictions	Sensor 1	Sensor 2
Incident Flux (w/cm^2)	10.39	
Average Radiance (w/cm^2 -sr)	3.31	28.07

Fig. 5 Concentric cylinder plume with different gas and particle temperatures in each region.

receiver was calculated using both a forward and a reverse Monte Carlo method. The results for the forward and reverse Monte Carlo methods were the same to within the statistical error of the Monte Carlo process as is shown in Table 2.

Additional test case results are presented for a plume that models the particle and gas temperature gradients in the plume flowfield as shown in Fig. 5. These results are included to enable others to compare to our results for a problem where the flowfield properties are well defined. In real plume flowfields, the properties are not well known, so it is hard to compare predictions and measurements. The model flowfield was composed of two concentric cylinders (50 and 80 cm in radius) with different particle and gas temperatures in each. The properties in each region are given in Fig. 5. The radiation from this plume was calculated for two sensors, both located 200-cm radially outward in the base plane of the plume. Sensor 1 had a FOV of 180 deg (full angle) and looked parallel to the plume centerline. Sensor 2 had a FOV of 2 deg (full angle) and looked downstream toward the plume at a 45-deg angle. The predicted average radiance for sensor 1 was 3.31 W/(cm^2-sr), while that for sensor 2 was 28.07 W/(cm^2-sr). Thus, sensor 2 with its 2-deg FOV would collect 0.0269 W/cm^2 of radiation.

Solid Rocket Motor Plume

Reverse Monte Carlo predictions for a typical solid rocket motor (SRM) plume are shown in Figs. 6–8. The plume flowfield was generated using the SPF code,[15] using methods described by Reardon et al.[16] The SRM had a contoured nozzle with an area ratio of 7.7 and an exit diameter of 70.3 cm. The propellant was ammonium perchlorate with 19% aluminum and 12% binder, which produced a plume containing H_2O, CO, CO_2, and HCl gases, and Al_2O_3 particles. The grain was an internal burning cylinder which produced a gradually increasing chamber pressure and a burn duration of about 30 s. The predictions are for a chamber pressure of 4086 KPa (590 psia) which occurs at about 5 s into the burn. Figure 6 shows a diagram of the plume. The shaded areas represent the gas temperature field. Superimposed on Fig. 6 are contours which indicate the position in the plume where the detected radiation originated. The radiation was detected by sensors (4-deg, full angle, FOV) that looked normal to the plume axis, across its diameter, at 1- and 6-nozzle exit radii downstream of the exit from a radial distance of 254 cm from the plume centerline. The long arrows in the figure represent the centerline of the sensor fields-of-view. The radiation source boundaries within the plume were determined from the coordinates of the endpoints of the absorbed rays. Using these coordinates, the average distance and the standard deviation of the average distance along the sensor line-of-sight were determined. These values defined the region's center and length. The region's width was defined as the average distance perpendicular to the sensor's line-of-sight for each ray endpoint. Figure 6 shows that most of the CO_2, 4.3-μm band radiation was emitted near the edge of the plume where the temperatures are 500–2500 K. Most of the particulate and H_2O gas radiation originates from near the plume center where the larger, hotter particles are located.

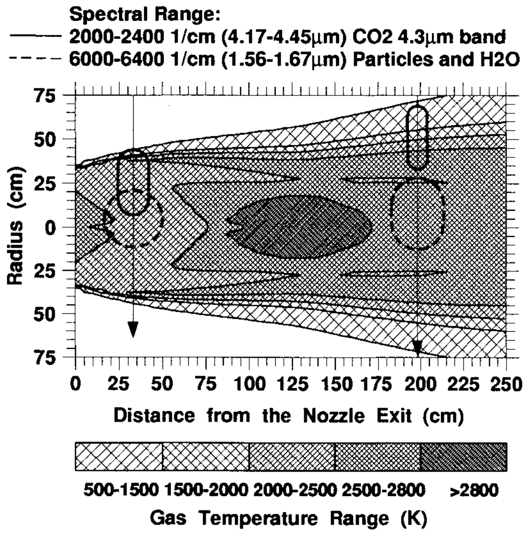

Fig. 6 Predicted SRM plume gas temperatures and regions of CO_2, H_2O, and Al_2O_3 radiation emission.

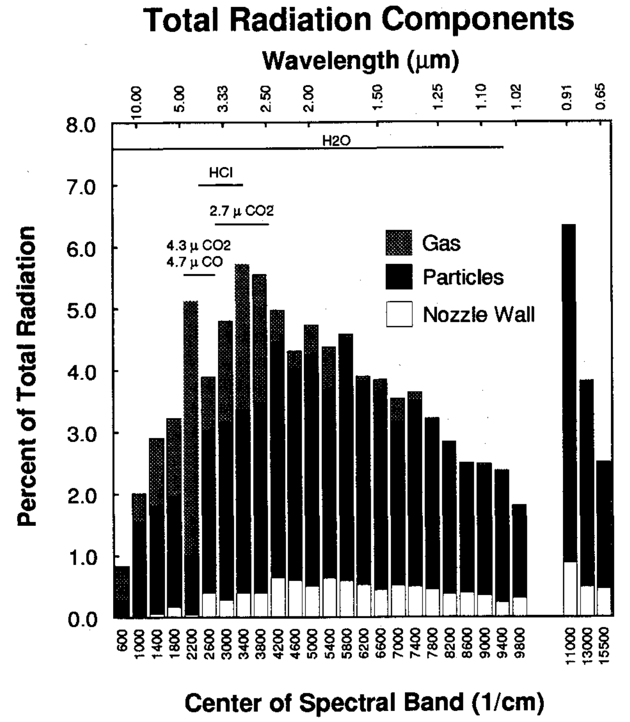

Fig. 7 Predicted SRM plume radiation spectra and emission sources 1-nozzle exit radius downstream. The integrated radiance is 28.1 W/cm^2-sr.

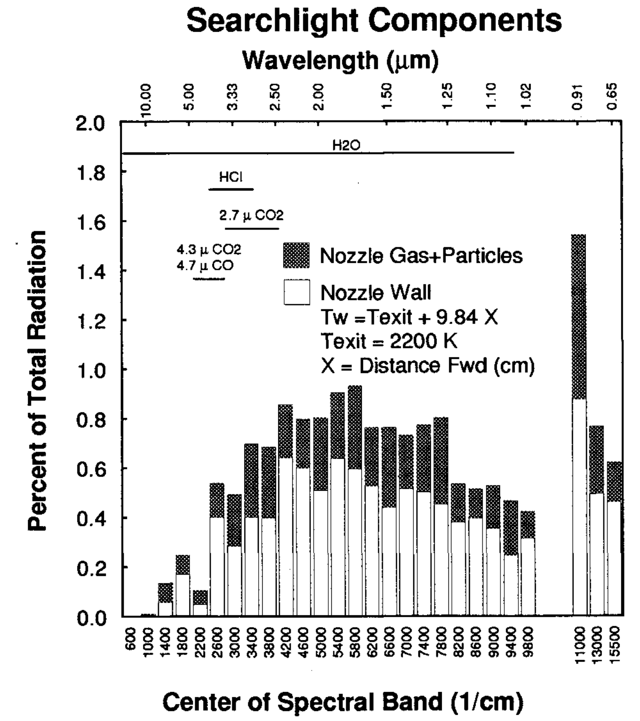

Fig. 8 Predicted SRM searchlight spectra and emission sources 1-nozzle exit radius downstream. Searchlight is 16.3% of the total radiation.

Figure 7 shows the predicted spectral distribution of the radiation detected by the sensor located 1-nozzle exit radii downstream. The total radiation detected by the sensor was 0.1075 W/(cm^2). The figure shows the percentage of total radiation in each spectral band as a function of the central wave number of the wave band. Note that the wavelength is given across the top of the figure. The wave bands for the far-IR, 400–10,000-cm^{-1} region, were each 400 cm^{-1}, the remaining three wave bands in the near-IR, and visible spectral region were from 10,000–12,000, 12,000–14,000 and 14,000–17,000 cm^{-1}. The spectral peak at 2200 cm^{-1} is due to the CO_2 4.3-μm band (1800–2400 cm^{-1}) and the CO 4.7-μm band (1400–2330 cm^{-1}) emission. The peak at 3400 cm^{-1} is the H_2O and CO_2 2.7-μm band (2400–4300 cm^{-1}).

Figure 7 also shows the sources of the radiation. The radiation originates either from the nozzle wall, the particles in the plume and the nozzle, or the gases in the plume and the nozzle. The Al_2O_3 particles radiate quite strongly compared to the gases across the entire spectral interval. They emit more radiation than the gases in each band except for the 2000–2400-cm^{-1} band, where CO_2 and CO gas emission is very strong. The high percentages in the near IR and visible spectra are due to the larger wave band intervals.

The searchlight component of the radiative heating is shown in Fig. 8. It includes all sources upstream of the nozzle exit plane, and therefore, includes some gas and particle sources as well as the nozzle wall. The nozzle wall temperature was assumed to increase as a function of distance into the nozzle, such that $T_w = 2200 + 9.84x$, where x is in cm and T_w is in K. The searchlight radiative heating is due mainly to the nozzle wall emission across the entire spectrum.

The computer time necessary for the calculations shown in Figs. 7 and 8 for the sensor located at 1-nozzle radius downstream, was 713 s. The time necessary to do the same calculations for the sensor located at 4-nozzle radii downstream was 625 s. The numerical calculations were done on a Sun/Spark workstation.

These examples provide an indication of the kind of diagnostic information that can be obtained from the reverse Monte Carlo method. Since each ray is followed through the plume (through successive scattering events to its final absorption), many other diagnostics are also possible and only need an indication of their usefulness to be implemented.

Conclusions

A reverse Monte Carlo code has been developed to predict radiative base heating due to rocket plumes. This code development is part of an ongoing program to improve the accuracy of radiative base heating predictions. The reverse Monte Carlo method is shown to work very well when one is interested in the radiation reaching a specific point. Very good agreement is achieved between the reverse Monte Carlo method and the forward Monte Carlo method for a pure scattering model plume, and between the reverse Monte Carlo method and the GASRAD code for a gas-only approximation of the SSME plume. Predictions for a typical absorbing, emitting, and scattering SRM plume are presented. It is shown that CO_2 emission near 2200 cm^{-1} occurs from near the outer edge of the plume; whereas, emission from H_2O gas and Al_2O_3 particles near 6200 cm^{-1} occurs from near the plume centerline. The emission spectra show that Al_2O_3 particles are responsible for most of the radiation over the 400–17,000-cm^{-1} spectral range. Searchlight and nozzle wall contribute a small, but nearly constant percentage, of the radiation over most of the spectral range.

The reverse Monte Carlo method is quite versatile. It can be applied to nonradially symmetric plumes and plumes with noncircular cross sections. It can also be applied to multiple plumes and account for gimbaled plume angles. Another complicated problem that can be addressed using the reverse Monte Carlo method is to include reflections off neighboring surfaces in the radiative transfer predictions.

Acknowledgments

This work was supported by NASA Marshall Space Flight Center, Huntsville, Alabama under Contract NAS8-39235, monitered by Peter Sulyma. The authors also wish to thank John E. Reardon of REMTECH, Inc. for his many helpful comments and suggestions.

References

[1] Reardon, J. E., and Lee, Y. C., "A Computer Program for Thermal Radiation from Gaseous Rocket Exhaust Plumes (GASRAD)," REMTECH, Inc., RTR 014-09, Huntsville, AL, Dec. 1979.

[2] Ludwig, C. B., Malkmas, W., Walker, J., Freeman, G. N., Reed, R., and Slack, M., "Standardized Infrared Radiation Model (SIRRM)," *Development and Validation*, Vol. 1; Air Force Rocket Propulsion Lab. TR-81-54, Edwards AFB, CA, 1981, pp. 101–106.

[3] Ludwig, C. B., Malkmus, W., Walker, J., Slack, M., and Reed, R., "A Theoretical Model for Absorbing, Emitting and Scattering Plume Radiation," *Spacecraft Radiative Transfer and Temperature Control*, edited by T. E. Horton, Vol. 83, Progress in Astronautics and Aeronautics, AIAA, New York, 1982, pp. 111–127.

[4] Markarian, P., and Kosson, R., "Standardized Infrared Radiation Model (SIRRM-II)," Vol. 1, Algorithm Upgrade Development, Air Force Astronautics Lab. TR-87-098, Edwards AFB, CA, March 1988.

[5] Watson, G. H., and Lee, A. L., "Solid Rocket Booster Thermal Radiation Model—Vol. 1—Final Report," Lockheed Missiles and Space Co., HREC TR D496763-1, Sunnyvale, CA, March 1976.

[6] Watson, G. H., and Lee, A. L., "Thermal Radiation Model for Solid Rocket Booster Plumes," *Journal of Spacecraft and Rockets*, Vol. 14, No. 11, 1977, pp. 641–647.

[7] Pearce, B. E., Wurster, W. H., Flanigan, M. C., Smolarek, K. K., and Huang, R., "Predictions and Measurements of Radiation Base Heating from a Solid Propellant Rocket Motor Plume," AIAA Paper 91-1431, June 1991.

[8] Vaughn, M. E., "SPF-II User Guide," U.S. Army Missile Command, Huntsville, AL, Sept. 1986.

[9] Nelson, H. F., "Modeling for Rocket Plume Base Heating Calculations," Chemical Propulsion Information Agency Publication 568, Columbia, MD, May 1991, pp. 585–592.

[10] Nelson, H. F., "Backward Monte Carlo Modeling for Rocket Plume Base Heating," *Journal of Thermophysics and Heat Transfer*, Vol. 6, No. 3, 1992, pp. 556–558.

[11] Reardon, J. E., Everson, J., Smith, S. D., and Sulyma, P. R., "ASRM Radiation and Flowfield Prediction Status," Chemical Propulsion Information Agency Publication 568, Columbia, MD, May 1991, pp. 537–547.

[12] Ludwig, C. B., Malkmus, W., Reardon, J. E., and Thompson, J. A. L., "Handbook of Infrared Radiation from Combustion Gases," Marshall Space Flight Center, NASA SP-3080, Huntsville, AL, 1973.

[13] Young, S. J., "Band Model Formulation for Inhomogeneous Optical Paths," *Journal of Quantitative Spectroscopy and Radiative Transfer*, Vol. 15, No. 6, 1975, pp. 483–501.

[14] Reardon, J. E., "Plume Radiation Measurements on the SSME Flight Nozzle," REMTECH Inc., RM 014-14, Huntsville, AL, March 1979.

[15] Smith, S. D., personal communication, SECA, Huntsville, AL, 1991.

[16] Reardon, J., Everson, J., and Smith, S. D., "Analytical Methodology for the Cycle 1.5 ASRB Plume Radiation Predictions," REMTECH Inc., RTN 250-1-02, Oct. 30, 1991.